

## Mössbauer and photocatalytic studies of CaFe<sub>2</sub>O<sub>4</sub> nanoparticle-containing aluminosilicate prepared from domestic waste simulated slag

ALI, AS, ISHIKAWA, S, NOMURA, K, KUZMANN, E, HOMONNAY, Z, SCRIMSHIRE, Alex <<http://orcid.org/0000-0002-6828-3620>>, BINGHAM, Paul <<http://orcid.org/0000-0001-6017-0798>>, KREHULA, S, RISTIĆ, M, MUSIĆ, S and KUBUKI, S

Available from Sheffield Hallam University Research Archive (SHURA) at:

<http://shura.shu.ac.uk/25052/>

---

This document is the author deposited version. You are advised to consult the publisher's version if you wish to cite from it.

### Published version

ALI, AS, ISHIKAWA, S, NOMURA, K, KUZMANN, E, HOMONNAY, Z, SCRIMSHIRE, Alex, BINGHAM, Paul, KREHULA, S, RISTIĆ, M, MUSIĆ, S and KUBUKI, S (2019). Mössbauer and photocatalytic studies of CaFe<sub>2</sub>O<sub>4</sub> nanoparticle-containing aluminosilicate prepared from domestic waste simulated slag. *Journal of Radioanalytical and Nuclear Chemistry*.

---

### Copyright and re-use policy

See <http://shura.shu.ac.uk/information.html>



24 **Keywords**

25 <sup>57</sup>Fe Mössbauer spectroscopy, Photocatalytic effect, Visible-light, Nanoparticles,  
26 CaFe<sub>2</sub>O<sub>4</sub>, α-Fe<sub>2</sub>O<sub>3</sub>,

27 **1. Introduction**

28 Treatments of waste materials and wastewater are serious environmental problems all  
29 over the world. The Organization for Economic Co-operation and Development (OECD)  
30 reported that the annual total amount of municipal waste discarded from the OECD  
31 affiliated countries was calculated to be  $6.22 \cdot 10^{11}$  kg, corresponding to the disposal of  
32 560 kg/person in 2007 [1]. These reported values concerning the amounts of waste  
33 materials are almost stable as compared with those recently reported values of  $6.56 \cdot 10^{11}$   
34 kg, corresponding 522 kg/person reported in 2013 [2]. As for the wastewater pollution in  
35 Japan, chemical oxidation demand (COD) achievement rate, which indicates the ratio of  
36 closed water system like pond or lake having the COD value less than the upper  
37 limitation of 8 mg L<sup>-1</sup> has been stable at around 55 % [3]. These statistics show that the  
38 no effective solutions for reducing the waste materials and for wastewater purification  
39 have been developed. Therefore, finding a new route for recycling solid waste as water  
40 purifying material is essential for solving serious environmental problems.

41 Our research group found that the glass-ceramics prepared from a domestic waste slag  
42 (WS), of which chemical component is SiO<sub>2</sub>(38.4 mass%), CaO(28.5), Al<sub>2</sub>O<sub>3</sub>(14.9),  
43 Fe<sub>2</sub>O<sub>3</sub>(5.5), and others (12.7), collected at the incineration plant in Ube city, Yamaguchi,  
44 Japan, with additional Fe<sub>2</sub>O<sub>3</sub> decreased the COD value from 250 to 36 mg L<sup>-1</sup> after 10  
45 days [4]. We then reported that iron-containing soda lime silicate glass with the chemical  
46 composition of 15Na<sub>2</sub>O•15CaO•(70-x)SiO<sub>2</sub>•xFe<sub>2</sub>O<sub>3</sub>, abbreviated as NCFSt, with 'x' of 50  
47 (in mass%) decreased COD value of artificial drain from 280 to 55.2 mg L<sup>-1</sup> after 10 days  
48 with the pseudo-first-order rate constant (*k*) of  $4.7 \cdot 10^{-1}$  day<sup>-1</sup>[5]. These results implied  
49 that the iron-silicate glass-ceramics could be applied as a water purifying materials for  
50 decomposing organic compounds which causes an increase in COD.

51 In relation to the development of wastewater purifying materials from iron silicate  
52 glass-ceramics, NCFS<sub>x</sub> glass with ‘x’ of 50 heat-treated at 1000 °C for 100 min  
53 decomposed methylene blue (MB) in the aqueous solution with the *k* of  $4.78 \cdot 10^{-4} \text{ min}^{-1}$   
54 [6]. The room temperature (RT) Mössbauer spectrum of the heat-treated NCFS<sub>x</sub> with  
55 ‘x’ of 50 were composed of an magnetic sextet with an isomer shift ( $\delta$ ) of  $0.36 \text{ mm s}^{-1}$   
56 and an internal magnetic field ( $H_{\text{int}}$ ) of 51.8 T due to hematite ( $\alpha\text{-Fe}_2\text{O}_3$ ) and a relaxed  
57 sextet with the  $\delta$  and  $H_{\text{int}}$  of  $0.34 \text{ mm s}^{-1}$  and 37.9 T, respectively, due to the iron oxide  
58 nanoparticles [6]. Further, a much larger *k* value of  $9.26 \cdot 10^{-3} \text{ min}^{-1}$  was recorded for MB  
59 decomposition test using a heat-treated  $15\text{Na}_2\text{O} \cdot 15\text{CaO} \cdot 40\text{Fe}_2\text{O}_3(30-x)\text{SiO}_2 \cdot x\text{Al}_2\text{O}_3$  glass,  
60 abbreviated as NCFSA<sub>x</sub> with ‘x’ of 11[7]. Two magnetic sextets with  $\delta$  and  $H_{\text{int}}$  of  $0.37$   
61  $\text{mm s}^{-1}$  and 51.2 T and  $0.38 \text{ mm s}^{-1}$  and 52.4 T were observed from the RT Mössbauer  
62 spectrum of this sample [7].

63 Recently, a glass-ceramics prepared from  $\text{Na}_2\text{CO}_3$ , WS and  $\text{Fe}_2\text{O}_3$ , abbreviated as  
64 NaWSF<sub>x</sub>, by melt-quenching method showed the *k* value of  $2.65 \cdot 10^{-3} \text{ min}^{-1}$  when they  
65 were heat-treated at 800 °C for 100 min [8]. The Mössbauer spectra measured at 77 K  
66 showed several sextets, one of which had  $\delta$  and  $H_{\text{int}}$  of  $0.41 \text{ mm s}^{-1}$  and 52.7 T attributed  
67 to nanoparticles of  $\alpha\text{-Fe}_2\text{O}_3$  [8]. These results show that the iron-containing silicates  
68 exhibit photocatalytic ability through the presence of  $\alpha\text{-Fe}_2\text{O}_3$  and its analogous iron  
69 oxides at the nano-scale. However, it is difficult for NaWSF<sub>x</sub> to precisely evaluate the  
70 visible light-activated photocatalytic effect of  $\alpha\text{-Fe}_2\text{O}_3$  precipitated in the silica glass  
71 matrix because WS contains lots of impurity elements.

72 Therefore, in order to classify the chemical environment of iron oxides which causes  
73 the visible-light activated photocatalytic activity in the silica matrix, the relationship  
74 between visible-light activated catalytic effects and local structure of “*simulated*”  
75 domestic waste slag with different iron concentrations, abbreviated as R-NaWSF<sub>x</sub> (*x* =  
76 10, 30 and 50 mass% of  $\text{Fe}_2\text{O}_3$  in the  $\text{Na}_2\text{O}\text{-CaO}\text{-SiO}_2\text{-Al}_2\text{O}_3\text{-Fe}_2\text{O}_3$  system) was  
77 investigated by  $^{57}\text{Fe}$ -Mössbauer spectroscopy, X-ray diffractometry(XRD), and  
78 ultraviolet-visible light absorption spectroscopy(UV-Vis).

79 **2. Experimental**

80 Glass and ceramics produced from domestic waste model slag with different iron  
 81 concentration, denoted as model-slag+10Na<sub>2</sub>O+xFe<sub>2</sub>O<sub>3</sub>, abbreviated as (R-NaWSF<sub>x</sub>,  $x =$   
 82 10, 30, 50 mass%) were prepared by melt quenching method. The chemical composition  
 83 of the model slag was based on the previously reported values[8] except for minor  
 84 components of the first transition metal oxides. Weighed amounts of Na<sub>2</sub>CO<sub>3</sub> (Wako  
 85 199-01585), CaCO<sub>3</sub> (Wako 030-00385), Fe<sub>2</sub>O<sub>3</sub> (Wako 096-04825), Al(OH)<sub>3</sub> (Wako 014-  
 86 01925) and SiO<sub>2</sub> (Kanto Kagaku 37974-00) were mixed with an agate mortar. The  
 87 mixture was put into a platinum crucible and melted at 1400 °C for 60 min in an electrical  
 88 muffle furnace. Dark brown samples were obtained by dipping the crucible bottom into  
 89 ice-cold water. The prepared glass and glass-ceramics were subjected to the following  
 90 isothermal heat treatment for 100 min at 800 and 900 °C. The estimated chemical  
 91 composition of R-NaWSF<sub>x</sub> is listed in Table 1.

92

93 **Table 1** The estimated chemical composition of R-NaWSF<sub>x</sub> (in wt%)

$x$	Na <sub>2</sub> O	CaO	Al <sub>2</sub> O <sub>3</sub>	SiO <sub>2</sub>	Fe <sub>2</sub> O <sub>3</sub>
10	11.2	26.9	14.0	23.3	24.6
30	9.6	23.1	12.0	20.0	35.3
50	8.4	20.2	10.5	17.5	43.4

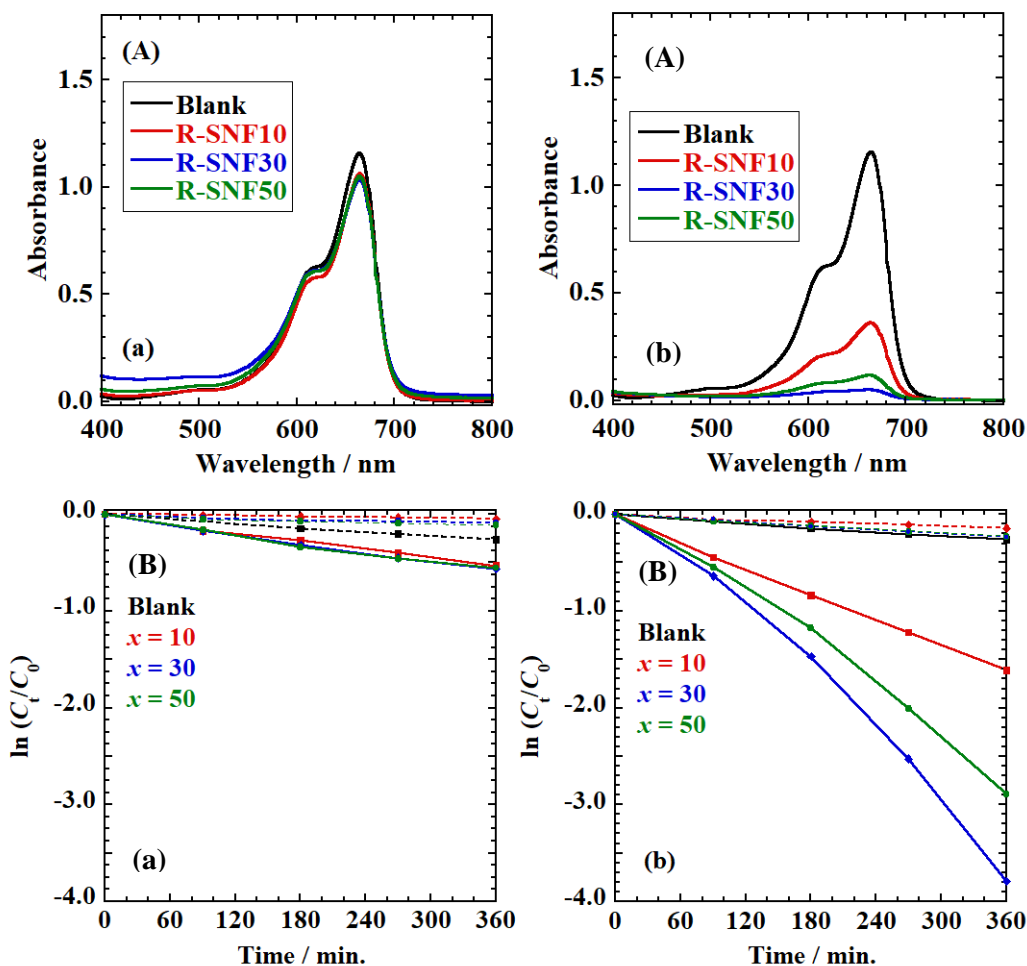
94

95 The prepared glasses and glass-ceramics containing model slag plus additions, before  
 96 and after heat-treatment were characterized by X-ray diffractometry (XRD), <sup>57</sup>Fe-  
 97 Mössbauer spectroscopy and ultra-violet visible-light absorption spectroscopy (UV-VIS).  
 98 The XRD patterns were measured in the  $2\theta$  range of 10 and 80 ° with the sampling pitch  
 99 of 0.02 ° and scan speed of 5 ° min<sup>-1</sup>. The X-rays of Cu-K<sub>α</sub> ( $\lambda = 0.1541$  nm) were  
 100 generated by applying the voltage of 50 kV and the current of 300 mA. The recorded  
 101 XRD patterns were identified by JCPDS cards by PDXL. Measurements of Mössbauer

102 spectra at room and liquid nitrogen temperatures (77 K) were carried out by conventional  
103 acceleration method using 925MBq  $^{57}\text{Co}(\text{Rh})$  and  $\alpha\text{-Fe}$  as a source and reference,  
104 respectively. For the measurement, 100 mg of well-pulverized sample is homogeneously  
105 dispersed on the transparent adhesive tape so that it was circular in shape with a diameter  
106 of 10 mm. The obtained spectra were fitted by Lorentzian lineshapes using Mosswinn  
107 3.0i XP software. For the evaluation of visible-light activated photocatalytic ability, 20  
108 mL of  $20\ \mu\text{mol L}^{-1}$  methylene blue aqueous solution ( $\text{MB}_{\text{aq}}$ ) prepared from methylene  
109 blue (Wako 133-06962) was poured into a plastic vial together with 40 mg of powdered  
110 sample, and irradiated with the visible light with the wavelength of 420 – 700 nm emitted  
111 from a metal halide lamp with an output power of 100 W and intensity of  $6\ \text{mWcm}^{-2}$ .  
112 The  $\text{MB}_{\text{aq}}$  concentration after the catalytic reaction was determined by UV-VIS  
113 spectrometer under the wavelength range of 200 – 800 nm and a scan speed of  $1\ \text{nm sec}^{-1}$ .

## 114 **3. Results and discussion**

### 115 **3.1 UV-VIS Spectra**



116  
 117 **Fig. 1** (A) UV-Vis spectra and (B)  $\ln(C_t/C_0)$  vs.  $t$  plot of  $MB_{aq}$  reacted with R-NaWSF<sub>x</sub>  
 118 after heat treatment for 100 min. at (a) 800 and (b) 900 °C

119 UV-Vis spectra of  $MB_{aq}$  degradation test using R-NaWSF<sub>x</sub> with 'x' of 10, 30 and 50  
 120 heat-treated for 100 min at 800 and 900 °C are shown in Fig. 1. We could confirm the  
 121 maximum absorption wavelength at 664 nm due to the original MB from the UV-Vis  
 122 spectra before the degradation test. The concentration of the  $MB_{aq}$  was determined by  
 123 the Lambert-Beer equation, *i.e.*,

$$124 \quad A = \varepsilon_0 C_t l \quad (1)$$

125 where  $A$ ,  $\varepsilon_0$ ,  $C_t$  and  $l$  are absorbance determined at 664 nm, molar absorption coefficient  
 126 ( $= 7.9 \cdot 10^4 \text{ mol}^{-1} \text{ cm}^{-1} \text{ L}[9]$ ), MB concentration after  $t$  min [ $\text{mol L}^{-1}$ ] and cell length ( $= 1$   
 127 cm), respectively. When the  $MB_{aq}$  was reacted in the dark with R-NaWSF<sub>x</sub> with  $x$  of 10,

128 30 and 50 after heat-treated at 800 °C for 100 min, almost constant MB concentration was  
 129 recorded for the degradation test using all three samples as shown in the dotted lines in  
 130 Fig. 1 (B) (a). On the other hand, a decrease in MB concentration was observed from  
 131 20.0 to 11.8, 11.4, and 12.8  $\mu\text{ mol L}^{-1}$  reacted under the visible-light with R-NaWSFex  
 132 having the 'x' of 10, 30 and 50 for 360 min, respectively ( see Fig. 1 (B) (a)). However,  
 133 the MB concentration after 360 min irradiation of visible-light was comparable to that of  
 134 a blank test (12.8  $\mu\text{ mol L}^{-1}$ ). In contrast, remarkable decreases in MB concentration  
 135 were observed from 20 to 4.00, 0.45, and 1.10  $\mu\text{ mol L}^{-1}$  by using R-NaWSFex with 'x'  
 136 of 10, 30 and 50 heat-treated at 900 °C, respectively ( see Fig. 1 (B) (b)).

137 A pseudo-first-order rate constant ( $k$ ) is evaluated by the following equation, *i.e.*,

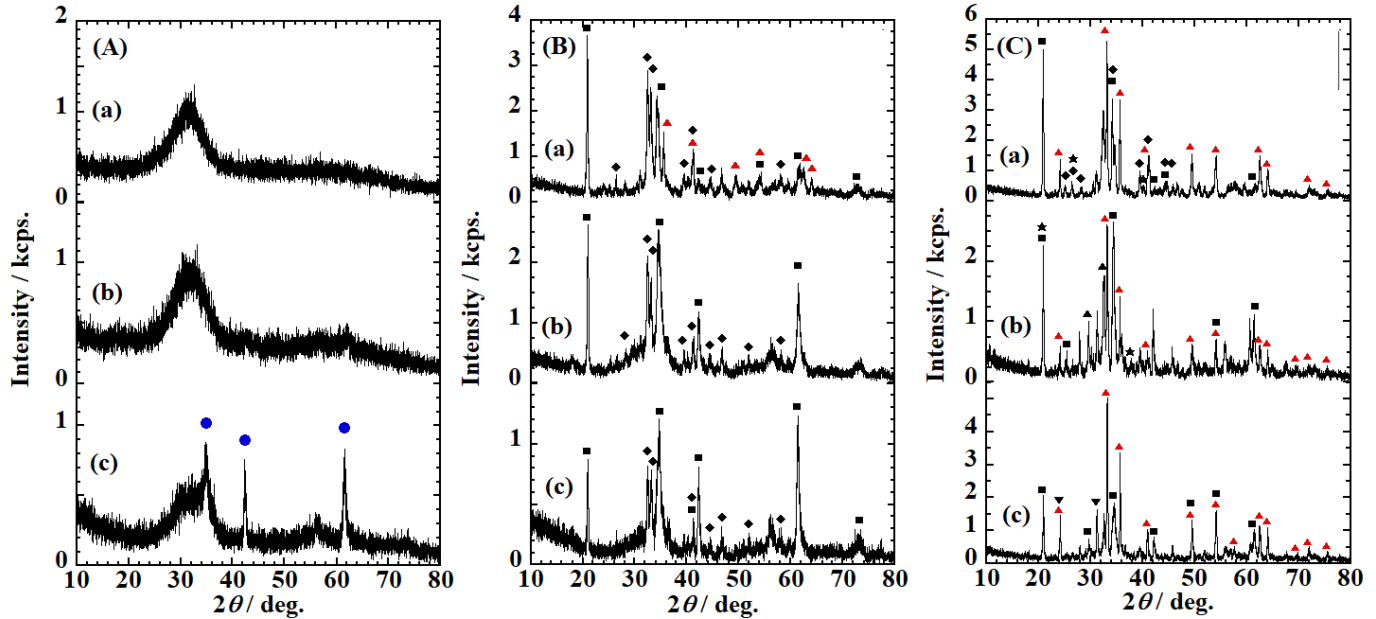
$$138 \quad \ln(C/C_0) = -kt \quad (2)$$

139 where  $C_0$  is the initial MB concentration ( = 20  $\mu\text{ mol L}^{-1}$ ). In order to evaluate the  
 140 photocatalytic ability of the studied samples, estimation of  $k$  values is carried out by  
 141 plotting,  $\ln(C/C_0)$  vs.  $t$ , as shown in Fig. 1(B). Under visible-light irradiation, almost  
 142 comparable  $k$  values of  $(1.48 \pm 0.02) \cdot 10^{-3}$ ,  $(1.63 \pm 0.01) \cdot 10^{-3}$  and  $(1.64 \pm 0.01) \cdot 10^{-3} \text{ min}^{-1}$   
 143 were respectively obtained for R-NaSWFex with 'x' of 10, 30 and 50 heat-treated for 100  
 144 min at 800 °C, which is slightly larger than that of blank value (=  $(1.20 \pm 0.01) \cdot 10^{-3} \text{ min}^{-1}$ ).  
 145 In contrast, much larger  $k$  values of  $(4.52 \pm 0.01) \cdot 10^{-3}$ ,  $(9.75 \pm 0.01) \cdot 10^{-3}$  and  
 146  $(7.59 \pm 0.01) \cdot 10^{-3} \text{ min}^{-1}$  were estimated for the same samples heat-treated for 100 min at  
 147 900 °C under the visible-light irradiation. These results indicate that R-NaWSFex heat-  
 148 treated at the higher temperature has a higher photocatalytic ability which depends on  
 149 kinds and amounts of the precipitated crystalline phases. In our previous study, we could  
 150 observe a  $k$  value of  $2.65 \cdot 10^{-3} \text{ min}^{-1}$  for a glass-ceramics prepared from  $\text{Na}_2\text{O}$ +domestic  
 151 waste slag+ $x\text{Fe}_2\text{O}_3$  by melting at 1400 °C for 1 h and heat-treated at 800 °C for 100 min  
 152 [8]. By comparing the largest  $k$  value obtained for R-NaWSFe30 heat-treated at 900 °C  
 153 in this study(= $9.75 \pm 0.01) \cdot 10^{-3} \text{ min}^{-1}$ ) and that obtained for the glass-ceramics prepared  
 154 from existing domestic waste slag(= $2.65 \cdot 10^{-3} \text{ min}^{-1}$ ), it can be said that much more  
 155 effective photocatalytic material can be prepared by isolating impurity from existing  
 156 domestic waste slag.



157

## 158 3.2 XRD patterns



159 **Fig. 2** XRD patterns of R-NaWSF<sub>x</sub> samples with 'x' of (a)10, (b) 30 and (c) 50, (A)  
 160 before and after heat treatment for 100 min at (B) 800 °C and (C) 900 °C. ●:  $\gamma$ -Fe<sub>2</sub>O<sub>3</sub>,  
 161 ■: NaAlSiO<sub>4</sub>, ◆: Ca<sub>2</sub>SiO<sub>4</sub>, ▲:  $\alpha$ -Fe<sub>2</sub>O<sub>3</sub>, ▲: Ca<sub>3</sub>SiO<sub>5</sub>, ▼: Ca<sub>2</sub>Al<sub>2</sub>SiO<sub>7</sub>, ★: SiO<sub>2</sub>.

162 In Fig. 2, XRD patterns of R-NaWSF<sub>x</sub> samples before and after heat treatment for 100  
 163 min at 800 °C and 900 °C are indicated. Before the heat treatment, we could confirm X-  
 164 ray halo patterns which have a peak at  $2\theta$  of around  $32.0^\circ$  due to the amorphous structure  
 165 for R-NaWSF<sub>x</sub> samples with 'x' of 10 and 30, whereas sharp intense peaks were  
 166 detected at the  $2\theta$  of  $34.8$ ,  $42.3$  and  $61.5^\circ$  due to maghemite ( $\gamma$ -Fe<sub>2</sub>O<sub>3</sub>, PDF No. 01-076-  
 167 4113) for R-NaWSFe50. The crystallite size ( $D$ ) of compounds detected by the XRD  
 168 patterns can be estimated by Sherrer's formula [10], *i.e.*,

$$169 \quad D = K\lambda / \beta \cos\Theta \quad (3)$$

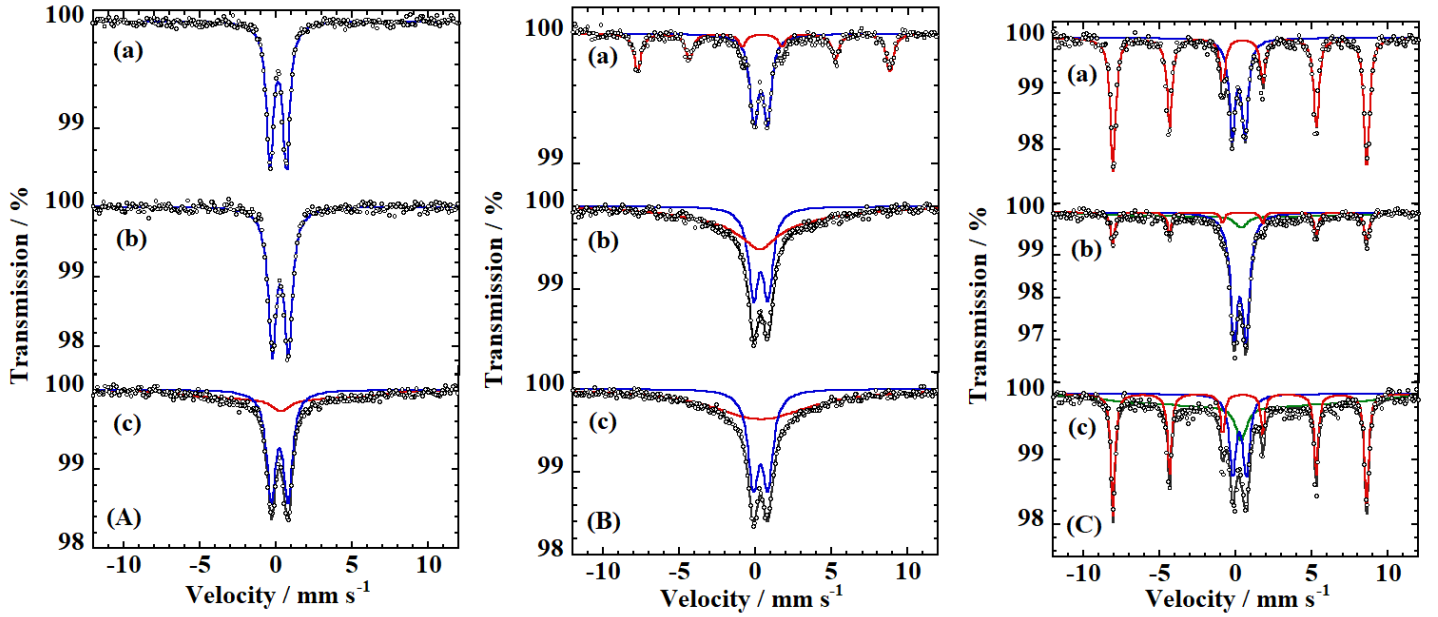
170 where  $K$ ,  $\lambda$  and  $\beta$  are Sherrer's constant, wavelength of the X-ray(= 0.1541 nm) and  
 171 full width at the half of maximum, respectively. Using the Sherrer's formula (3), the  
 172 crystallite size of  $\gamma$ -Fe<sub>2</sub>O<sub>3</sub> precipitated in R-NaWSFe50 was calculated to be  $(24\pm 9)$  nm.

173 It should be noted that the thermal stability of R-NaWSF<sub>x</sub> becomes higher because XRD  
174 pattern of glass-ceramics prepared from as collected domestic waste slag with similar  
175 chemical composition showed peaks due to the crystalline phase when it contains  
176 additional Fe<sub>2</sub>O<sub>3</sub> of more than 30 mass% [8]. As for XRD patterns of R-NaWSF<sub>x</sub>  
177 samples after heat-treatment at 800 °C, crystalline phases of NaAlSiO<sub>4</sub> (PDF No. 00-011-  
178 0221) and Ca<sub>2</sub>SiO<sub>4</sub> (PDF No. 01-086-0399) were identified in all samples, while α-  
179 Fe<sub>2</sub>O<sub>3</sub> (PDF No. 01-089-0599) can be identified only in the case of  $x = 10$ . After heat-  
180 treatment at 900 °C, α-Fe<sub>2</sub>O<sub>3</sub> can be detected in all samples with additional phases of  
181 SiO<sub>2</sub> (PDF No. 01-089-8937) for  $x = 10$  and 30, while for  $x = 50$ , Ca<sub>2</sub>Al<sub>2</sub>SiO<sub>7</sub> (PDF No.  
182 01-075-1677) can be detected. The averaged crystallite sizes were respectively estimated  
183 to be  $29 \pm 4$ ,  $35 \pm 5$  and  $25 \pm 3$  nm for  $x = 10$ , 30 and 50 heat-treated at 800 °C, while  
184 they were  $47 \pm 5$ ,  $44 \pm 4$  and  $41 \pm 3$  nm for 900 °C heat-treated samples. When we  
185 consider the differences in the  $k$  values of  $1.48\text{-}1.64 \cdot 10^{-3} \text{ min}^{-1}$  observed for MB<sub>aq</sub>  
186 degradation test using R-NaWSF<sub>x</sub> heat-treated at 800 °C and those of  $4.52 \cdot 10^{-3}$ -  
187  $9.75 \cdot 10^{-3} \text{ min}^{-1}$  recorded by using samples after heat-treated at 900 °C, it can be  
188 considered that precipitation of α-Fe<sub>2</sub>O<sub>3</sub> phase is essential for exhibiting visible-light  
189 activated photocatalytic effect of heat-treated R-NaWSF<sub>x</sub>.

190

### 191 3.3 <sup>57</sup>Fe-Mössbauer Spectra

#### 192 3.3.1 Room temperature (RT) <sup>57</sup>Fe-Mössbauer Spectra



193 **Fig. 3** RT Mössbauer spectra of R-NaWSF<sub>x</sub> sample with 'x' of (a) 10, (b) 30, and (c) 50  
 194 (A) before and after heat treatment for 100 min at (B) 800 °C, and (C) 900 °C

195

196 **Table 2** <sup>57</sup>Fe-Mössbauer parameters of R-NaWSF<sub>x</sub> sample with 'x' of 10, 30, 50 before  
 197 and after heat treatment for 100 min at 800 °C, and 900 °C for 100 min

	$x$	Assignment	$A$ %	$\delta$ $\text{mm s}^{-1}$	$\Delta$ $\text{mm s}^{-1}$	$H_{\text{int}}$ T	$\Gamma$ $\text{mm s}^{-1}$
Before	10	Fe <sup>III</sup> ( $T_d$ )	100	$0.15_{\pm 0.01}$	$1.06_{\pm 0.01}$	—	$0.55_{\pm 0.01}$
	30	Fe <sup>III</sup> ( $T_d$ )	100	$0.29_{\pm 0.01}$	$1.04_{\pm 0.01}$	—	$0.64_{\pm 0.01}$
	50	Fe <sup>III</sup> ( $T_d$ )	59.5	$0.25_{\pm 0.01}$	$1.10_{\pm 0.02}$	—	$0.68_{\pm 0.02}$
		Fe <sup>III</sup> ( $O_h$ )M	40.5	$0.37_{\pm 0.01}$	$0.00_{\pm 0.01}$	$37.0_{\pm 2.6}$	$0.99_{\pm 0.30}$
800	10	Fe <sup>III</sup> ( $T_d$ )	56.3	$0.34_{\pm 0.01}$	$0.88_{\pm 0.01}$	—	$0.62_{\pm 0.01}$
		Fe <sup>III</sup> ( $O_h$ )	43.7	$0.49_{\pm 0.01}$	$0.10_{\pm 0.02}$	$51.4_{\pm 0.1}$	$0.54_{\pm 0.03}$
	30	Fe <sup>III</sup> ( $T_d$ )	38.3	$0.34_{\pm 0.01}$	$0.95_{\pm 0.01}$	—	$0.76_{\pm 0.03}$
		Fe <sup>III</sup> ( $T_d$ )	61.7	$0.27_{\pm 0.12}$	$0.00_{\pm 0.01}$	$48.0_{\pm 0.1}$	$1.83_{\pm 0.88}$
	50	Fe <sup>III</sup> ( $T_d$ )	38.2	$0.34_{\pm 0.01}$	$0.95_{\pm 0.01}$	—	$0.82_{\pm 0.03}$
		Fe <sup>III</sup> ( $T_d$ )	61.8	$0.37_{\pm 0.01}$	$0.00_{\pm 0.01}$	$48.2_{\pm 0.1}$	$7.71_{\pm 0.96}$
900	10	Fe <sup>III</sup> ( $T_d$ )	30.3	$0.19_{\pm 0.01}$	$0.83_{\pm 0.01}$	—	$0.49_{\pm 0.01}$

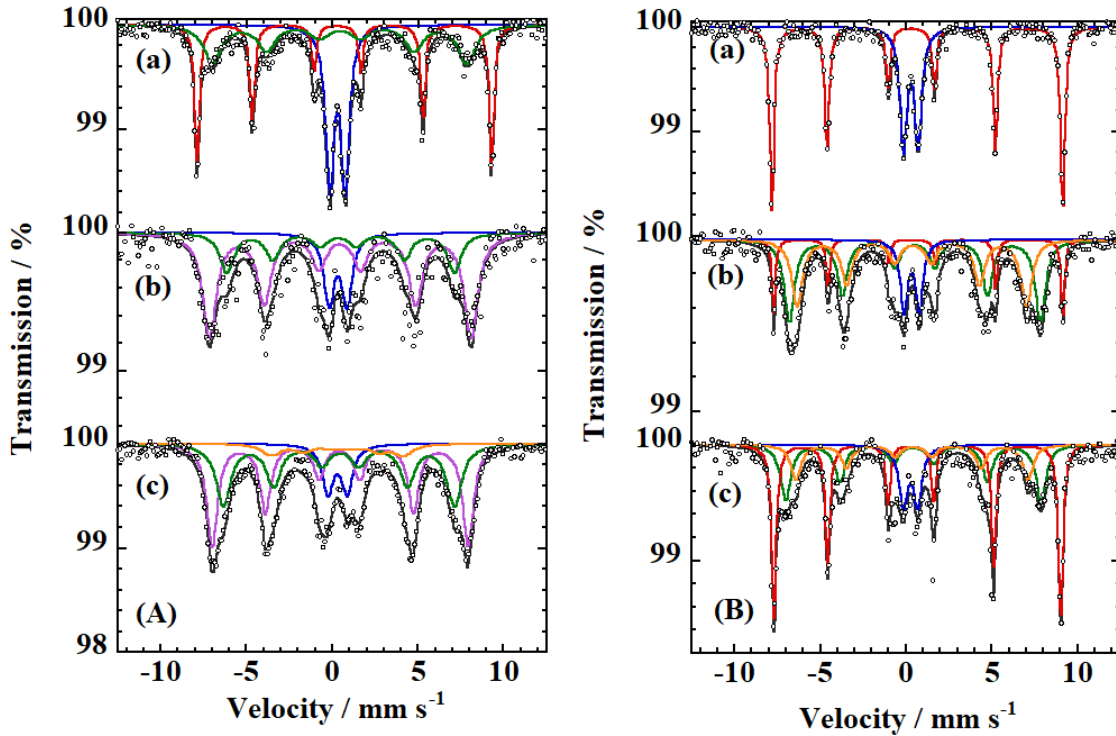
		$\text{Fe}^{\text{III}}(O_{\text{h}})\text{H}$	69.7	$0.38_{\pm 0.01}$	$-0.20_{\pm 0.01}$	$51.6_{\pm 0.02}$	$0.40_{\pm 0.01}$
	30	$\text{Fe}^{\text{III}}(T_{\text{d}})$	58.1	$0.29_{\pm 0.01}$	$0.78_{\pm 0.01}$	—	$0.58_{\pm 0.01}$
		$\text{Fe}^{\text{III}}(O_{\text{h}})\text{H}$	16.3	$0.37_{\pm 0.01}$	$-0.20_{\pm 0.01}$	$51.7_{\pm 0.05}$	$0.30_{\pm 0.02}$
		$\text{Fe}^{\text{III}}(O_{\text{h}})\text{H}$	25.6	$0.37_{\pm 0.01}$	$-0.20_{\pm 0.01}$	$51.2_{\pm 0.01}$	$0.29_{\pm 0.01}$
	50	$\text{Fe}^{\text{III}}(T_{\text{d}})$	20.1	$0.26_{\pm 0.01}$	$0.89_{\pm 0.02}$	—	$0.51_{\pm 0.03}$
		$\text{Fe}^{\text{III}}(O_{\text{h}})\text{H}$	37.3	$0.38_{\pm 0.01}$	$-0.20_{\pm 0.01}$	$51.7_{\pm 0.02}$	$0.31_{\pm 0.01}$
		$\text{Fe}^{\text{III}}(O_{\text{h}})\text{H}$	42.6	$0.37_{\pm 0.01}$	$-0.20_{\pm 0.01}$	$50.2_{\pm 1.91}$	$0.31_{\pm 0.07}$

198 A: absorption area ( $\pm 0.5$  %), M:  $\gamma\text{-Fe}_2\text{O}_3$ , H:  $\alpha\text{-Fe}_2\text{O}_3$

199

200  $^{57}\text{Fe}$ -Mössbauer spectra recorded at room temperature and the corresponding  
 201 parameters of R-NaWSFex sample before and after heat-treatment for 100 min at 800 °C  
 202 and 900 °C were shown in Fig. 3 and Table 2, respectively. As shown in Fig. 3 (A) (a)-  
 203 (c),  $^{57}\text{Fe}$ -Mössbauer spectra of R-NaWSFex before the heat treatment are composed of  
 204 one paramagnetic doublet with an isomer shift ( $\delta$ ) of  $(0.15 \pm 0.01) - (0.25 \pm 0.01)$  mm s<sup>-1</sup>  
 205 <sup>1</sup> and quadrupole splitting ( $\Delta$ ) of  $(1.04 \pm 0.01) - (1.10 \pm 0.02)$  mm s<sup>-1</sup> due to distorted  
 206  $\text{Fe}^{\text{III}}\text{O}_4$  tetrahedra. An additional relaxed component with  $\delta$  of  $(0.37 \pm 0.01)$  mm s<sup>-1</sup> and  
 207 an internal magnetic field ( $H_{\text{int}}$ ) of  $(37.0 \pm 2.6)$  T due to iron oxide nanoparticles was  
 208 observed for R-NaWSFe50 (Fig. 3 (A) (c)). The  $^{57}\text{Fe}$ -Mössbauer spectrum of R-  
 209 NaWSFe10 after heat treatment for 100 min at 800 °C indicated one paramagnetic  
 210 doublet due to distorted  $\text{Fe}^{\text{III}}\text{O}_4$  and a magnetic sextet with  $\delta$  of  $(0.49 \pm 0.01)$  mm s<sup>-1</sup>,  $H_{\text{int}}$   
 211 of  $(51.4 \pm 0.1)$  T and  $\Gamma$  of  $(0.54 \pm 0.03)$  mm s<sup>-1</sup> due to regular  $\alpha\text{-Fe}_2\text{O}_3$ . A sextet with  
 212 similar parameters attributed to  $\alpha\text{-Fe}_2\text{O}_3$  were observed for all the Mössbauer of R-  
 213 NaWSFex heat-treated at 900 °, as shown in Fig. 3 (C) (a)-(c). These results are  
 214 consistent with those of corresponding XRD patterns. However, there are several  
 215 components which are not clearly identified for the crystalline phase of iron oxide.  
 216 Therefore, low-temperature Mössbauer measurement was required in order to  
 217 characterize these components.

218

219 3.3.2 LNT  $^{57}\text{Fe}$ -Mössbauer Spectra

220

221 **Fig. 4** Mössbauer spectra measured at 77 K of R-NaWSF<sub>x</sub> sample with 'x' of (a) 10, (b)  
 222 30 and (c) 50 after heat treatment for 100 min at (A) 800 °C and (B) 900 °C

223 **Table 3** Mössbauer parameters at 77 K of R-NaWSF<sub>x</sub> sample after heat treatment for  
 224 100 min at 800 °C and 900 °C

	$x$	Assignment	$A$ %	$\delta$ $\text{mm s}^{-1}$	$\Delta$ $\text{mm s}^{-1}$	$H_{\text{int}}$ T	$\Gamma$ $\text{mm s}^{-1}$
800	10	$\text{Fe}^{\text{III}}(T_{\text{d}})$	32.1	$0.29_{\pm 0.01}$	$0.90_{\pm 0.01}$	—	$0.56_{\pm 0.02}$
		$\text{Fe}^{\text{III}}(O_{\text{h}})\text{H}$	34.9	$0.49_{\pm 0.01}$	$0.39_{\pm 0.01}$	$53.4_{\pm 0.1}$	$0.33_{\pm 0.01}$
		$\text{Fe}^{\text{III}}(O_{\text{h}})$	33.0	$0.44_{\pm 0.03}$	$-0.04_{\pm 0.06}$	$46.1_{\pm 0.1}$	$1.20_{\pm 0.10}$
	30	$\text{Fe}^{\text{III}}(T_{\text{d}})$	15.2	$0.32_{\pm 0.03}$	$1.04_{\pm 0.05}$	—	$0.70_{\pm 0.10}$
		$\text{Fe}^{\text{III}}(O_{\text{h}})\text{C}$	61.8	$0.44_{\pm 0.02}$	$0.03_{\pm 0.04}$	$47.4_{\pm 0.1}$	$0.95_{\pm 0.07}$
		$\text{Fe}^{\text{III}}(T_{\text{d}})$	23.1	$0.42_{\pm 0.05}$	$0.13_{\pm 0.01}$	$41.1_{\pm 0.05}$	$0.95_{\pm 0.02}$
	50	$\text{Fe}^{\text{III}}(T_{\text{d}})$	10.7	$0.31_{\pm 0.02}$	$1.12_{\pm 0.04}$	—	$0.77_{\pm 0.06}$
		$\text{Fe}^{\text{III}}(O_{\text{h}})\text{C}$	45.0	$0.43_{\pm 0.01}$	$0.03_{\pm 0.02}$	$46.4_{\pm 0.1}$	$0.75_{\pm 0.04}$

		Fe <sup>III</sup> ( $T_d$ )	36.2	$0.43_{\pm 0.02}$	$-0.10_{\pm 0.04}$	$41.9_{\pm 0.2}$	$1.01_{\pm 0.07}$
		Fe <sup>III</sup> ( $T_d$ )	8.1	$0.43_{\pm 0.01}$	$-0.22_{\pm 0.24}$	$24.0_{\pm 0.7}$	$1.27_{\pm 0.4}$
900	10	Fe <sup>III</sup> ( $T_d$ )	32.7	$0.28_{\pm 0.01}$	$0.86_{\pm 0.01}$	-	$0.48_{\pm 0.02}$
		Fe <sup>III</sup> ( $O_h$ )H	67.3	$0.47_{\pm 0.01}$	$0.35_{\pm 0.01}$	$52.7_{\pm 0.1}$	$0.32_{\pm 0.01}$
	30	Fe <sup>III</sup> ( $T_d$ )	12.1	$0.33_{\pm 0.02}$	$0.90_{\pm 0.03}$	-	$0.50_{\pm 0.04}$
		Fe <sup>III</sup> ( $O_h$ )H	13.0	$0.52_{\pm 0.01}$	$0.37_{\pm 0.02}$	$52.4_{\pm 0.1}$	$0.25_{\pm 0.02}$
		Fe <sup>III</sup> ( $O_h$ )C	40.5	$0.51_{\pm 0.01}$	$-0.01_{\pm 0.02}$	$45.5_{\pm 0.1}$	$0.71_{\pm 0.05}$
		Fe <sup>III</sup> ( $T_d$ )	34.4	$0.37_{\pm 0.02}$	$-0.08_{\pm 0.03}$	$41.5_{\pm 0.2}$	$0.75_{\pm 0.06}$
	50	Fe <sup>III</sup> ( $T_d$ )	12.6	$0.26_{\pm 0.03}$	$0.84_{\pm 0.04}$	-	$0.60_{\pm 0.07}$
		Fe <sup>III</sup> ( $O_h$ )H	42.1	$0.46_{\pm 0.01}$	$0.38_{\pm 0.01}$	$52.0_{\pm 0.1}$	$0.32_{\pm 0.02}$
		Fe <sup>III</sup> ( $O_h$ )C	27.7	$0.44_{\pm 0.02}$	$-0.02_{\pm 0.05}$	$46.3_{\pm 0.2}$	$0.69_{\pm 0.07}$
		Fe <sup>III</sup> ( $T_d$ )	17.6	$0.39_{\pm 0.04}$	$-0.10_{\pm 0.07}$	$42.0_{\pm 0.1}$	$0.69_{\pm 0.07}$

225 A: absorption area ( $\pm 0.5$  %), H:  $\alpha$ -Fe<sub>2</sub>O<sub>3</sub>, C: CaFe<sub>2</sub>O<sub>4</sub>

226 <sup>57</sup>Fe-Mössbauer spectra measured at 77 K and the corresponding parameters for R-  
227 NaWSFex sample with 'x' of 10, 30 and 50 heat-treated for 100 min at 800 °C and 900 °C  
228 are indicated in Fig. 4 and Table 3, respectively. When in the case of the 77 K <sup>57</sup>Fe-  
229 Mössbauer spectrum of R-NaSWFe10 heat-treated at 800 °C, one paramagnetic doublet  
230 with  $\delta$  of  $(0.29 \pm 0.01)$  mm s<sup>-1</sup> and  $\Delta$  of  $(0.90 \pm 0.01)$  mm s<sup>-1</sup> due to Fe<sup>III</sup>O<sub>4</sub> tetrahedra  
231 substituting for Si<sup>IV</sup>O<sub>4</sub>, and two sextets with  $\delta$  and  $H_{int}$  of  $(0.49 \pm 0.01)$  mm s<sup>-1</sup> and  $(53.4$   
232  $\pm 0.1)$  T due to  $\alpha$ -Fe<sub>2</sub>O<sub>3</sub>, and  $(0.44 \pm 0.03)$  mm s<sup>-1</sup> and  $(46.1 \pm 0.1)$  T iron oxide  
233 nanoparticles were observed. It is noted that the positive  $\Delta$  value of  $(0.39 \pm 0.01)$  mm s<sup>-1</sup>  
234 observed for 77 K Mössbauer spectrum of R-NaWSFe10 is due to Morin transition  
235 occurred at 260 K[11], which is also confirmed for 77 K Mössbauer spectrum of R-  
236 NaWSFe heat-treated at 900 °C indicating the existence of  $\alpha$ -Fe<sub>2</sub>O<sub>3</sub> in the XRD patterns  
237 (Fig. 2 (C)). In addition to a paramagnetic component and two magnetic sextets observed  
238 in the 77 K Mössbauer spectrum of R-NaWSFe10, additional one sextet was observed for  
239 LNT Mössbauer spectrum of NaWSFe30, and two sextets for NaWSFe50, respectively.

240 On the other hand, a paramagnetic doublet with  $\delta$  of  $(0.26 \pm 0.03) - (0.33 \pm 0.02)$  mm s<sup>-1</sup>  
241 <sup>1</sup> and  $\Delta$  of  $(0.84 \pm 0.04) - (0.90 \pm 0.03)$  mm s<sup>-1</sup> due to Fe<sup>III</sup>O<sub>4</sub> tetrahedra and a magnetic  
242 sextet with  $\delta$  of  $(0.46 \pm 0.01) - (0.51 \pm 0.02)$  mm s<sup>-1</sup>, internal magnetic field ( $H_{\text{int}}$ ) of  $(52.0$   
243  $\pm 0.1) - (52.7 \pm 0.1)$  T and line width ( $I$ ) of  $(0.25 \pm 0.02) - (0.32 \pm 0.02)$  mm s<sup>-1</sup> due to  $\alpha$ -  
244 Fe<sub>2</sub>O<sub>3</sub> were commonly found for Mössbauer spectra of R-NaWSFex heat-treated at 900  
245 °C measured at 77 K. The larger  $H_{\text{int}}$  value obtained in this study is caused by weak  
246 ferromagnetic interaction due to lowering of Morin transition temperature. A similar  
247 Mössbauer spectrum with  $\delta$  of 0.49 mm s<sup>-1</sup> and  $H_{\text{int}}$  of 53.5 T measured at 4.2 K was  
248 previously reported for  $\alpha$ -Fe<sub>2</sub>O<sub>3</sub> with the particle size of smaller than 20 nm [12]. In  
249 addition to these two components, two magnetic sextets with  $\delta$  and  $H_{\text{int}}$  of  $(0.51 \pm 0.01)$   
250 mm s<sup>-1</sup> and  $(45.5 \pm 0.1)$  T due to CaFe<sub>2</sub>O<sub>4</sub>[13], and  $(0.37 \pm 0.02)$  mm s<sup>-1</sup> and  $(41.5 \pm 0.2)$   
251 T due to iron oxide nanoparticles with unknown structure are observed for 77 K  
252 Mössbauer spectrum of R-NaWSFe30 heat-treated at 900 °C. Smaller absorption area  
253 ( $A$ ) of 27.7 % due to CaFe<sub>2</sub>O<sub>4</sub> and 17.6 % of unknown iron oxide nanoparticles were  
254 observed for 77 K Mössbauer spectrum of R-NaWSFe50 heat-treated at 900 °C. In the  
255 evaluation of  $k$  values for the MB decomposition by using heat-treated R-NaWSFex, the  
256 largest value of  $(9.75 \pm 0.01) \cdot 10^{-3}$  min<sup>-1</sup> was obtained when R-NaWSFe30  
257 heat-treated at 900 °C was used. It was reported that the band gap energy of CaFe<sub>2</sub>O<sub>4</sub> of  
258 1.85-1.90 eV[14,15] is slightly smaller than that of  $\alpha$ -Fe<sub>2</sub>O<sub>3</sub>(1.9-2.2 eV)[16,17]. By  
259 considering together this information with the above-described results of Mössbauer and  
260 UV-Vis studies, it can be said that the existence of nanoparticles of CaFe<sub>2</sub>O<sub>4</sub> cause the  
261 increase of  $k$  value in addition to  $\alpha$ -Fe<sub>2</sub>O<sub>3</sub>. It is concluded that iron oxide nanoparticles  
262 precipitated in aluminosilicate are essential for exhibiting visible-light activated  
263 photocatalytic effect.

## 264 Conclusions

265 The largest pseudo-first-order rate constant ( $k$ ) of  $9.75 \cdot 10^{-3}$  min<sup>-1</sup> was recorded for  
266 methylene blue degradation test by using R-NaWSFe30 heat-treated at 900 °C for 100  
267 min under visible-light irradiation. 77 K <sup>57</sup>Fe-Mössbauer spectrum of this sample

268 revealed the existence of nanoparticles of  $\text{CaFe}_2\text{O}_4$ , which was essential for the visible-  
269 light activated photocatalytic effect. It is concluded that visible-light activated  
270 photocatalyst can be prepared from ubiquitous elements of Na, Al, Si, O, Ca, and Fe.  
271 This paper implies that solid waste such as domestic slag which contains above-described  
272 elements can be recycled as wastewater purifying material in the future.

## 273 **Acknowledgments**

274 Some of the authors (ASA, SI, KN, and SK) express their gratitude for the financial  
275 support from Tokyo Human Resources Fund for City Diplomacy.

## 276 **References**

- 277 [1] OECD (2010) “Municipal waste” in OECD Factbook 2010: Economic,  
278 Environmental and Social Statistics. OECD Publishing, Paris. DOI:  
279 10.1787/factbook-2010-en.
- 280 [2] OECD (2016) “Municipal waste” in OECD Factbook 2015-2016: Economic,  
281 Environmental and Social Statistics. OECD Publishing, Paris. DOI:  
282 10.1787/factbook-2015-en.
- 283 [3] Annual Report on the Environment, the Sound Material-Cycle Society and  
284 Biodiversity in Japan 2018. <http://www.env.go.jp/en/wpaper/2018/pdf/07.pdf>,  
285 Accessed 1 July 2019
- 286 [4] Kubuki S, Kawakami N, Kamikawa T, Fukagawa M, Nishizumi T, Nishida T,  
287 Homonnay Z, Kuzmann E (2005) Corelationship between local structure and water  
288 purifying ability of iron-containing waste glasses. *Hyperfine Interact.* 166: 429-436
- 289 [5] Kubuki S, Iwanuma J, Akiyama K, Homonnay Z, Kuzmann E, Nishida T (2013)  
290 Water cleaning ability and local structure of iron-containing soda-lime silicate glass.  
291 *Hyperfine Interact.* 218:41-45.
- 292 [6] Kubuki S, Iwanuma J, Takahashi Y, Akiyama K, Homonnay Z, Sinkó K,



- 293 Kuzmann E, Nishida T (2014) Visible light-activated catalytic effect of iron-  
294 containing soda-lime silicate glass characterized by  $^{57}\text{Fe}$ -Mössbauer spectroscopy. J.  
295 Radioanal. Nucl. Chem. 301:1–7
- 296 [7] Iida Y, Akiyama K, Kobzi B, Sinkó K, Homonnay Z, Kuzmann E, Ristić M,  
297 Krehula S, Nishida T, Kubuki S (2015) Structural analysis and visible light-activated  
298 photocatalytic activity of iron-containing soda-lime aluminosilicate glass. J. Alloys  
299 Comp. 645:1–6
- 300 [8] Ishikawa S, Kobzi B, Sunakawa K, Nemeth S, Lengyel A, Kuzmann E, Homonnay  
301 Z., Nishida T, Kubuki S (2017) Visible-light activated photocatalytic effect of glass  
302 and glass-ceramic prepared by recycling waste slag with hematite. Pure Appl. Chem.  
303 89(4): 535-544
- 304 [9] Wakasa M, Kobayashi Y, Okano M (2006) Magnetic Field Effect on the  
305 Photocatalytic Reaction with  $\text{TiO}_2$  Semiconductor Film. Bull. Soc. Sci. Photo. Jpn.  
306 69(4) 271-275 (in Japanese)
- 307 [10] Scherrer P (1918) Bestimmung der Größe und der inneren Struktur von  
308 Kolloidteilchen mittels Röntgenstrahlen. Göttinger Nachrichten Gesell. 2:98-100  
309 (in Germany)
- 310 [11] F. Van der Wurde (1967) Mössbauer effect in  $\alpha\text{-Fe}_2\text{O}_3$ . Physica Status Solidi (b)  
311 17(1): 417- 432
- 312 [12] Murad E, Johnston J. H. (1984) In: Long G. J. (ed) Mössbauer Spectroscopy Applied  
313 to Inorganic Chemistry, Vol. 2, Plenum Press, New York, pp. 523-531
- 314 [13] Hirabayashi D, Sakai Y, Yoshikawa T, Mochizuki K, Kojima Y, Suzuki K, Ohshita  
315 K, Watanabe Y (2006) Mössbauer characterization of calcium-ferrite oxides  
316 prepared by calcining  $\text{Fe}_2\text{O}_3$  and CaO. Hyperfine Interact. 167(1-3):809-813
- 317 [14] Matsumoto Y, Omae M, Sugiyama K, Sato E. I (1987) New photocathode materials  
318 for hydrogen evolution:  $\text{CaFe}_2\text{O}_4$  and  $\text{Sr}_7\text{Fe}_{10}\text{O}_{22}$ . J. Phys. Chem. 91(3): 577–581
- 319 [15] Matsumoto Y, Sugiyama K, Sato E. I (1988) Improvement of  $\text{CaFe}_2\text{O}_4$  photocathode  
320 by doping with Na and Mg. J. Solid State Chem. 74(1): 117–125

321 [16] Sivula K, Le Formal F, Grätzel M (2011) Solar Water Splitting: Progress Using  
322 Hematite ( $\alpha$ -Fe<sub>2</sub>O<sub>3</sub>) Photoelectrodes. *ChemSusChem*, 4: 432–449.

323 [17] Iandolo B, Wickman B, Zorić I, Hellman A (2015) The Rise of Hematite: Origin and  
324 Strategies to Reduce the High Onset Potential for the Oxygen Evolution Reaction. *J.*  
325 *Mater. Chem. A* 3: 16896– 16912.

326

327

328